Unified picture of the photoexcitations in phenylene-based conjugated polymers: Universal spectral and dynamical features in subpicosecond transient absorption

B. Kraabel, V. I. Klimov, R. Kohlman, S. Xu, H-L. Wang, and D. W. McBranch
Chemical Science and Technology Division, CST-6, MS-J585, Los Alamos National Laboratory, Los Alamos, New Mexico 87545
(Received 8 October 1999)

Using subpicosecond transient absorption spectroscopy, we investigate the primary photoexcitations in thin films and solutions of several phenylene-based conjugated polymers and an oligomer. We identify several features in the transient absorption spectra and dynamics that are common to all of the materials which we studied from this family. The first spectral feature is a photoinduced absorption (PA) band peaking near 1 eV that has intensity-dependent dynamics that match the stimulated emission dynamics exactly over two orders of magnitude in excitation density. This band is associated with singlet intrachain excitons. The second spectral feature (observed only in thin films and aggregated solutions) is a PA band peaking near 1.8 eV, that is longer lived than the 1 eV exciton PA band, and that has dynamics that are independent (or weakly dependent) on excitation density. This feature is attributed to polarons, generated through a mechanism that is sample dependent. In pristine samples, polarons are generated via a mechanism that is quadratic in exciton density, whereas in photodegraded samples or samples doped with electron acceptors, the generation mechanism becomes linear in exciton density.

I. INTRODUCTION

Conjugated polymers, most notably those belonging to the poly(para-phenylenevinylene) (PPV) family, are technologically promising materials due to the ease with which they may be processed and the wide range over which their optical and electronic properties may be chemically tuned. Over the last decade numerous potential technological applications have been demonstrated, including electroluminescent devices (light-emitting diodes[1,2] and light-emitting electrochemical cells[3]), solid-state lasers,[4–6] photodetectors,[7,8] photovoltaic devices,[9] transistors,[10,11] and integrated optoelectronic devices.[12,13] All of these technologies would benefit from a unified picture of the fundamental photophysics of conjugated polymeric solids, and although many groups have contributed towards this goal,[14–32] there is still not widespread agreement about such a general framework.

Transient absorption (TA) spectroscopy is a powerful tool for studying the fundamental photophysics of conjugated polymers, but the interpretation of TA experiments has been the subject of much debate.[14] The transient photoinduced absorption (PA) features observed in PPV and its derivatives have been attributed variously to triplet excitons,[15] polarons,[27] singlet intrachain excitons[26] (also referred to as ''singlet polaron excitons''),[30,33] spatially indirect excitons (also referred to as polaron pairs),[20,21,23,24,30] and biexcitons.[19,31] More recently, the species previously referred to as spatially-indirect excitons (polaron pairs) have been assigned by some authors as excimers.[34–36] In addition to the controversy over the nature of the fundamental photoexcitations, there is also significant disagreement over what conditions govern the branching between different excitations, and whether various photoexcitations are photo-generated directly or in secondary processes. Site-selective fluorescence measurements[37] and photoluminescence quantum efficiency measurements[38] suggest that in excess of 90% of the initial photoexcitations in thin films of some PPV derivatives (including unsubstituted PPV and cyano-substituted PPV) are singlet intrachain excitons. In studies of different PPV derivatives (MEH-PPV), other authors have concluded that only about 10% of the initial photoexcitations are singlet excitons, with the majority being generated as spatially-indirect excitons[21,24] or excimers.[35] Several factors contribute to the disparity in experimental results, including widely varying experimental conditions for each particular measurement (e.g. excitation density, wavelength, or polarization of the photoexciting light), and the fact that the samples under study have varied considerably in fundamental ways, such as chemical structure and morphology (e.g., solutions, films cast from various solvents, or thermally converted, insoluble films), or the degree of photochemical degradation.

While it would clearly be desirable to have similar experimental conditions for all TA measurements of PPV derivatives, this is not the case for the large volume of literature cited above, due principally to the continually evolving nature of pulsed laser technology. It is now well established that the photoexcitation density is a crucial parameter in TA measurements,[29] since the decay dynamics in both solid samples and solutions vary strongly with changing excitation density, through a combination of nonlinear decay mechanisms[29,33,39–42] and nonlinear generation mechanisms.[30,31]

The degree of photochemical degradation of the sample also is known to be an important factor in determining the types of photoexcitations created and the relaxation pathways for these photoexcitations. The degradation has been attributed to scission of the conjugated chain (at the vinylene double bond) with corresponding formation of terminal carbonyl and aldehyde groups[24,26,33,43,44] as a result of photo-oxidation or high-temperature thermal conversion. The formation of these defects destroys the extended conjugation of the polymer chains, and thereby eliminates the strong $\pi - \pi^*$ absorption. In addition, these defects act as efficient

quenching centers for singlet excitons, since the electronegative carbonyl group is a strong electron acceptor, leading to the dissociation of the exciton.[24]

Another factor to consider in interpreting the various TA measurements is the effect of the substituent groups that are added to the PPV backbone in order to improve solubility or to tune the electronic properties of the material.[45–47] The effect of substituent groups on the electronic properties of these materials may be considerable, e.g., shifting the ground-state absorption and excited-state absorption and emission spectra dramatically[48] and independently,[21] so that some derivatives display stimulated emission, while others may not. The substituent groups also play a role in determining the morphology of samples, which strongly affects the optical and electronic properties of solid films.[49] Substituent groups may be added symmetrically or asymmetrically to the polymer backbone, with a dramatic influence on the degree of aggregation in the sample, the microscopic interchain packing density and the degree of crystallinity.[50,51] For a given PPV derivative, solid samples cast from different solvents, or from solutions of different concentrations, may have quite different morphological structure.[36,52,53] Finally, even assuming that one uses the same PPV derivative and attempts to account for other experimental variables, experience has shown that different batches of the ''same'' polymer can give somewhat different results.[26]

In light of the diversity of experimental results in the literature, and the multitude of experimental factors responsible for this diversity, there is a critical need for a more general description of the fundamental photophysics in phenylene-based conjugated polymers–*a description that applies to all members of this important class of materials*. In this paper, we report detailed spectral TA measurements of a number of PPV derivatives in various morphologies, and discuss their common features and a simple framework for understanding their properties, which is general to the entire class of phenylene-based conjugated materials. The materials studied include several soluble PPV derivatives in either spun-cast film or solution-aggregate form, self-assembled films of thermally-converted PPV, a PPV oligomer, and films of poly(9,9-dioctylfluorene) (PFO).

In all of these materials, we find evidence of two different types of photoexcitations, singlet intrachain excitons and charge-separated excitations. The singlet intrachain excitons give rise to stimulated emission in the visible regime and a pair of excited-state PA bands in the near-infrared, with dynamics that are strongly dependent on the initial excitation density. The PA signature of the charge-separated excitations is remarkably general to all the materials studied in our laboratory to date, and consists of a PA band which peaks in the red region of the visible spectrum, between the near-IR PA peak and the SE peak of the singlet exciton. The dynamics of the charge-separated species are essentially independent of the initial excitation density. In pristine polymers, the generation mechanism is a quadratic process, whereas in doped polymers it becomes a linear process. Several different species, including excimers, polaron pairs, or excitons that undergo dissociative electron transfer to electron-accepting defects or dopants, may all contribute to this photoinduced absorption, in proportions that are dependent on extrinsic factors such as sample morphology, excitation density and the degree of sample photochemical degradation. However, in light of the remarkable similarity of the PA signature across a range of different phenylene-based conjugated polymers, and, most importantly, between pristine samples and deliberately doped samples, we believe that TA in the red region of the spectrum is primarily due to polarons (unbound charged carriers on the polymer).

II. EXPERIMENT

PFO films were prepared in an argon atmosphere by spin-coating from a 3×10^{-2}-M chloroform solution onto sapphire substrates. Thermal annealing of the films resulted in samples that displayed some degree of aggregation (as deduced from changes to the linear absorption spectra[53]) but no difference was found in the TA spectra or dynamics between the ''aggregated'' and ''nonaggregated'' samples. Multilayered thin films of a water-soluble cationic PPV precursor polymer were prepared by ionic self-assembly with alternating layers of a transparent anionic polymer [poly(styrene sulfonate)].[54] The films were subsequently thermally converted to fully conjugated, insoluble PPV films.[54] Two soluble derivatives of PPV, poly(2-methyl-5-propyloxysulfonate phenylene vinylene) (MPS-PPV) and poly(2,3-diphenyl-5-hexyl-*p*-phenylene vinylene) (DP6-PPV) were also studied. Solutions of MPS-PPV were prepared in an N_2 atmosphere at a concentration of 10^{-3}–10^{-4} M in deionized water, and the solutions were bubbled with N_2 for one hour. Thin films of DP6-PPV were made by spin coating onto sapphire substrates from a chloroform solution (5×10^{-3} M). Approximately seven layers of DP6-PPV were applied, spinning each layer at 1000 RPM for 30 seconds in order to obtain an optical density of $\sim$0.5 at the pump wavelength, and a typical film thickness of $\sim$150 nm. All of the processing for the DP6-PPV films was done in an argon atmosphere, including transferring the films into an optical cryostat, in order to minimize the effects of photochemical degradation. We also study blends of DP6-PPV with cholestanoxy methanofullerene[55] (C_{60}) in a 1:1 molar ratio. The same precautions against photochemical degradation were taken for these samples as for the pristine samples of DP6-PPV. We also compare our results with those published previously using the model oligomer 2-methoxy-5-(2U-ethylhexyloxy)-distyryl benzene (MEH-DSB).[30,31] Solutions of this oligomer were prepared using *p*-xylenes as a solvent, and thin films ($\sim$100 nm) were prepared by vacuum sublimation onto sapphire substrates, then transferred into an optical cryostat in an argon atmosphere.

The chemical structure of each material is shown in Fig. 1, and their linear absorption spectra are shown in Fig. 2. With the exception of the PFO measurements, which were carried out in air, all measurements were carried out under a dynamic vacuum of 10^{-5} torr. The TA signals were monitored for signs of photodegradation (manifested as a gradual, irreversible decrease in TA signal) and all results reported here are for samples that did not photodegrade during the measurement. In some cases, samples contained a large concentration of exciton-trapping defects (due to thermal conversion, inherent impurities, or deliberate photo-oxidation) with dramatic results on TA spectra and dynamics. However, our procedure ensured that the degree of degradation did not

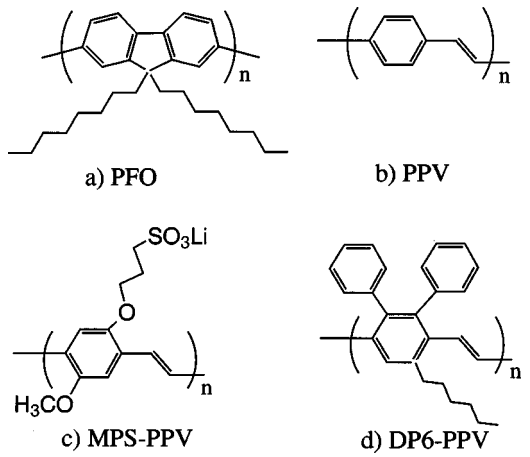

FIG. 1. The chemical structure for the materials discussed in this work: (a) PFO, (b) PPV, (c) MPS-PPV and (d) DP6-PPV.

change significantly during a given TA measurement.

The experimental setup used for the chirp-free transient absorption measurements has been described in detail elsewhere.[56] We emphasize that the instrumentation allows for compensation of the dispersion (chirp) of the probe pulse, so that all spectral measurements reported here are free from artifacts due to the chirp of the probe pulse. The samples were photoexcited at 3.1 eV, within the $\pi-\pi^*$ absorption band for all the materials used in this study (see Fig. 2). All samples were optically thin, so that the excitation density was approximately uniform throughout the sample. Cross-correlation measurements between the pump and the probe using two-photon absorption in a sapphire plate showed a system resolution time of 150 fs over the entire spectral range studied.[56] As a measure of transmission changes we use the differential transmission (DT), which is defined as $DT=(T-T_0)/T_0=\Delta T/T_0$, where T_0 and T are the transmission of the probe beam in the presence and absence of the pump, respectively. The pump-induced absorption change $\Delta\alpha$ is related to DT by the expression $\Delta\alpha=-1/d\ln(1+DT)$ where d is the sample thickness. In the small-signal regime in which we are operating, $\Delta\alpha d\sim-\Delta T/T_0$. Unless otherwise stated, all measurements reported here were taken with the pump beam polarized parallel to the probe beam.

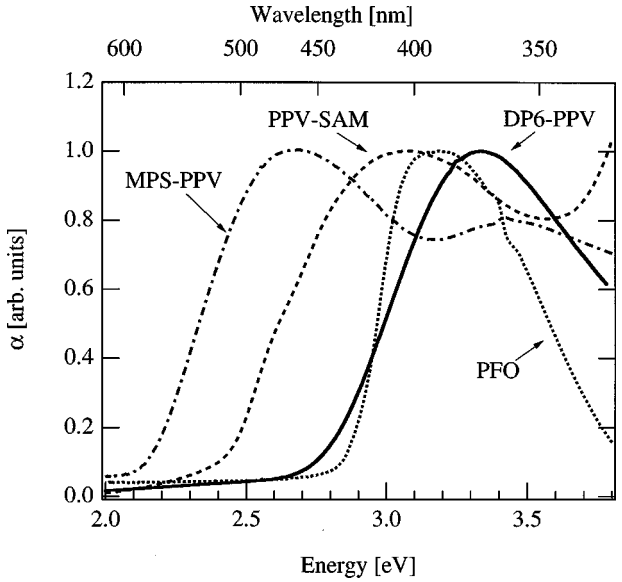

FIG. 2. The linear absorption spectra of the materials discussed in this work.

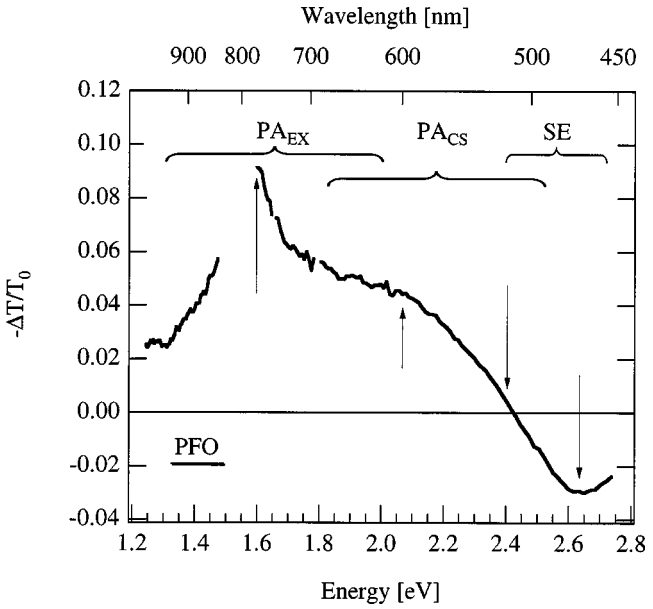

FIG. 3. The chirp-free transient absorption spectrum of oriented PFO at a 0.1 ps pump-probe delay time with a pump fluence of 10^{15} cm^{-2}. The arrows indicate the energy at which the measurements of the dynamics and pump-fluence dependence were made. The spectral regions corresponding to PA_{EX}, PA_{CS}, and the SE are also indicated.

III. RESULTS

A. PFO films

Figure 3 shows the chirp-free TA spectrum for a PFO thin film at a pump-probe delay time of 0.1 ps photoexcited with a pump fluence of $10^{15}\,cm^{-2}$. The spectrum consists of a region of negative $\Delta\alpha$ at energies above $\sim$2.4 eV, and a broad, positive $\Delta\alpha$ (PA) band from 2.4 eV to 1.2 eV. Since the negative $\Delta\alpha$ band occurs within the optical gap for this material (in a region with no ground-state absorption), we attribute this band to stimulated emission (SE). Within the PA band, two spectral features can be distinguished, labeled in Fig. 3 as PA_{EX} (peaking at $\sim$1.6 eV), and PA_{CS} (peaking near 2.1 eV).

The dynamics of the PA_{EX}, PA_{CS}, and SE bands for PFO at two different excitation densities are plotted in Fig. 4. Figure 4(a) shows the dynamics at a pump fluence of 10^{14} cm^{-2} for SE (solid circles) and PA_{EX} (solid line), and also the dynamics at a pump fluence of $10^{15}\,cm^{-2}$ for SE (open circles) and PA_{EX} (dashed line). The SE dynamics correspond closely to those of PA_{EX} at both excitation densities, demonstrating that the same species is responsible for both PA_{EX} and SE, namely the intrachain singlet exciton. The dynamics of this species depend strongly on the excitation density. At low pump fluences ($10^{13}\,cm^{-2}$) the long term dynamics appear exponential with a time constant of approximately 500 ps; the limited signal-to-noise ratio at these low fluences prevents a more precise determination. Upon

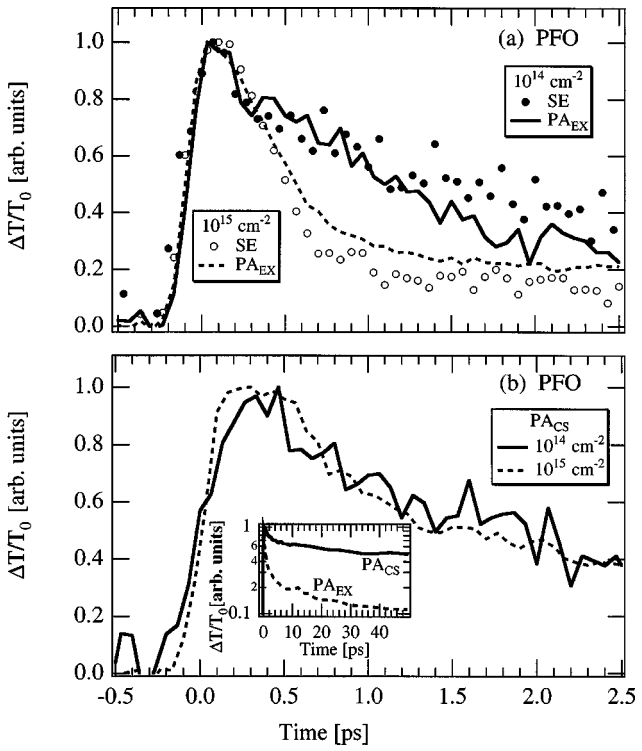

FIG. 4. Panel (a) shows the dynamics of the SE (solid circles) and PA_{EX} (solid line) for a pump fluence of $10^{14}\,cm^{-2}$ for unoriented PFO. The open circles and dashed line show the dynamics for the SE and PA_{EX}, respectively, for a pump fluence of $10^{15}\,cm^{-2}$. Panel (b) shows the dynamics of PA_{CS} for a pump fluence of 10^{14} (solid line) and $10^{15}\,cm^{-2}$ (dashed line), for unoriented PFO. The inset to panel (b) shows the dynamics of PA_{EX} (dashed line) and of PA_{CS} (solid line) in oriented PFO at a pump fluence of $10^{15}\,cm^{-2}$.

increasing the pump fluence above $10^{14}\,cm^{-2}$, a fast component appears in the dynamics. In this excitation density regime, the early time dynamics (<10 ps) can be characterized using a double exponential with time constants of roughly 500 fs and 5 ps.

The dynamics of the PA_{CS} feature in PFO are shown in Fig. 4(b) for pump fluences of $10^{14}\,cm^{-2}$ (solid line) and 10^{15} (dashed line) cm^{-2}. The results clearly show that the dynamics are independent of excitation density over this range. We also note that the dynamics for PA_{CS} are slower than those observed for PA_{EX} [see inset to Fig. 4(b)], implying that the species responsible for PA_{CS} is longer lived than the singlet intrachain exciton.

The dependence on pump fluence of the peak TA signal for PA_{CS} and PA_{EX} is shown in Fig. 5. PA_{EX} is linear in excitation density at low pump fluence, and saturates at higher pump fluences. In order to estimate the pump fluence at which saturation occurs, the data may be fit using

$$TA(\Phi)\propto(1-e^{-\Phi/\Phi_0}), \tag{1}$$

where Φ represents the pump fluence and Φ_0 the saturation fluence. The fit is shown as the thin dotted line in Fig. 5 and yields a saturation fluence of $\sim 10^{15}\,cm^{-2}$.

The thick solid line in Fig. 5 is the (scaled) result of squaring the data for PA_{EX}. This line matches exactly the data for PA_{CS}, showing that the generation mechanism for

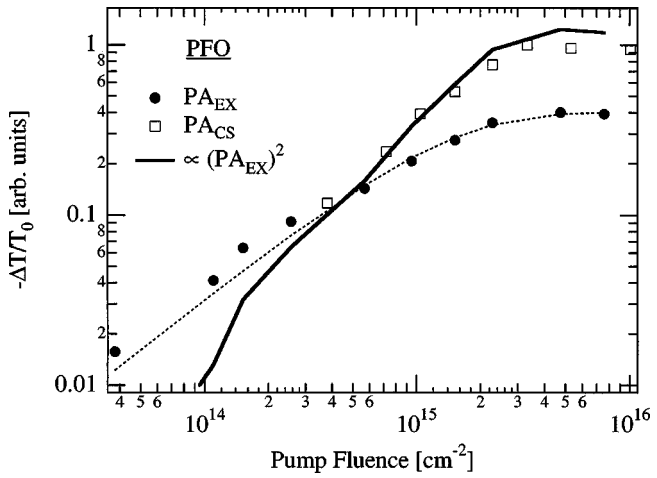

FIG. 5. The pump-fluence dependence of PA_{EX} (solid circles) and of PA_{CS} (open squares) in PFO at the peak of the TA signal. The heavy solid line is the (scaled) square of the data for PA_{EX}, and the thin-dashed line is a fit using Eq. (1), and yields a saturation fluence of $\sim 10^{15}\,cm^{-2}$.

PA_{CS} is exactly quadratic in the singlet exciton population, both above and below the saturation limit for singlet excitons.

Figure 6 shows the growth dynamics of PA_{CS} along with the dynamics of PA_{EX}, inverted and scaled to highlight the fact that the initial fast decay of PA_{EX} is complementary to the growth of PA_{CS}, implying that the PA_{CS} forms at the expense of PA_{EX}. Since it is necessary to measure the rise-time of PA_{CS} near the zero crossing of the TA spectrum (to avoid spectral overlap from PA_{EX}), in order to obtain a reasonable signal-to-noise ratio the risetime dynamics were obtained using pump fluences approaching the saturation fluence (this is true for all the pristine materials we discuss here). For the purpose of characterizing the rise-time of

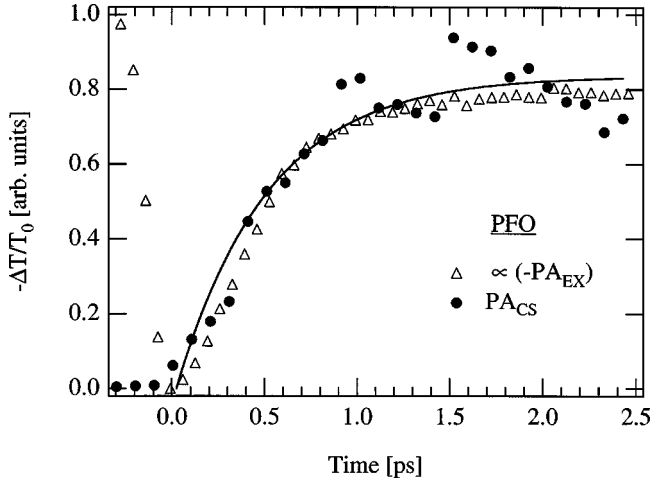

FIG. 6. The growth dynamics of PA_{CS} (solid circles) and the decay dynamics of PA_{EX} (open triangles) in PFO for a pump fluence of $10^{15}\,cm^{-2}$. The decay dynamics have been inverted and scaled to highlight the complementary dynamics between the growth of the PA_{CS} and the decay of PA_{EX}. The thin-solid line is a momoexponential fit to the growth dynamics of PA_{CS} and yields a time constant of ~ 500 fs.

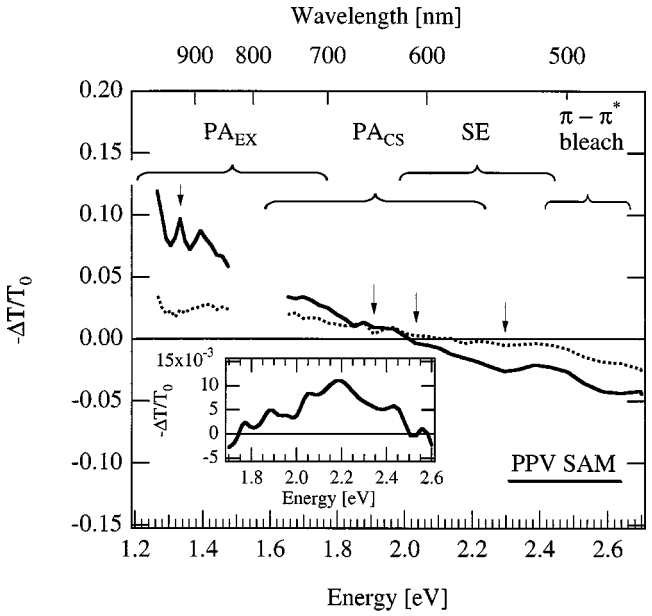

FIG. 7. The chirp-free transient absorption spectrum for PPV self-assembled monolayers at 0.1 (solid line) and 2 ps (dashed line) pump-probe delay time for a pump fluence of $10^{14}\,\mathrm{cm}^{-2}$. The arrows mark the regions where the dynamics were measured; the general features PA_{EX}, PA_{CS}, and the SE are also indicated. The inset shows the difference spectrum which is the result of scaling the 50 ps spectrum so that it matches the 0.1 ps spectrum at the $\pi-\pi^*$ bleach, then subtracting the 0.1 ps spectrum from the (scaled) 50 ps spectrum.

PA_{CS}, we fit the data to a monoexponential (thin soid line in Fig. 6) and obtain $\tau_{rise}=500$ fs.

The spectral features, their dependence on pump fluence, their intensity-dependent dynamics and the complemenatry growth time of PA_{CS} with respect to PA_{EX} are qualitatively very similar to what was reported in thin films of MEH-DSB,[30,31] indicating that the fundamental photophysics of the two materials are closely related.

B. PPV self-assembled multilayers

The chirp-free TA spectra for PPV self-assembled multilayers (SAMs) at 0.1 and 2 ps pump-probe delay time are shown in Fig. 7 using a pump fluence of $\sim 10^{14}\,\mathrm{cm}^{-2}$. Again, the spectra show a region of negative $\Delta\alpha$ above approximately 2.0 eV at early pump-probe delay times, and a region of positive $\Delta\alpha$ below 2.0 eV. Since the optical gap for PPV is about 2.4 eV, we attribute the negative $\Delta\alpha$ above 2.4 eV to bleaching of the $\pi-\pi^*$ transition, and the negative $\Delta\alpha$ from 2.0 to 2.4 eV to SE.

The positive TA spectrum in PPV SAMs shows less structure than is observed in either PFO or MEH-DSB. However, the general shape is similar, consisting of a broad spectral feature which peaks near 1.2 eV with a shoulder from 1.6 to approximately 2.0 eV. This additional broadening of the PA bands is consistent with the increased degree of structural disorder expected due to the relatively large number of defects and resulting large distribution of conjugation lengths known to exist in PPV films prepared by this method.[24] However, two distinct spectral regions within this broad PA band can be identified by examining their different intensity-dependent dynamics at various spectral energies. As before, these regions are marked PA_{EX} (the near-IR feature peaking near 1.2 eV) and PA_{CS} (energies near 1.9 eV intermediate between PA_{EX} and the SE). The probe energies at which detailed dynamics and pump-fluence dependence measurements were taken for these two features are indicated in Fig. 7 by arrows.

Unlike what is observed in PFO films and in MEH-DSB dilute solutions, in PPV SAM's the PA_{CS} band competes with the SE, as demonstrated by the fact that the zero crossing point of the TA spectrum shifts in time from approximately 2.0 eV at zero pump-probe delay to around 2.5 eV at a delay of 50 ps after photoexcitation. A similar ''dynamic blueshift'' of the TA spectrum zero crossing has been reported before in thin films of at least two PPV derivatives.[22,28,33] This provides clear evidence that a species different from the singlet intrachain exciton is present in increasingly large proportion to the exciton population, giving rise to a PA_{CS} band that directly overlaps and competes with the SE. This competing PA band can be clearly seen in the inset to Fig. 7. The data in the inset depicts the TA difference spectrum, calculated by first scaling the 50 ps spectrum so that its magnitude matches that of the 0.4 ps spectrum at 2.5 eV (the spectral position of the peak $\pi-\pi^*$ bleach), then subtracting the 0.4 ps spectrum from the scaled 50 ps spectrum. The difference spectrum shows that at long delay times, a secondary PA band dominates the TA spectrum. This spectrum is strikingly similar to the PA_{CS} spectrum that can be directly observed (due to greater spectral separation between PA_{CS} and SE) in PFO, MEH-DSB films, and photodegraded or fullerene-doped DP6-PPV (see below).

The dynamics of these different spectral features in PPV SAM's are depicted in Fig. 8 for various excitation densities. The SE dynamics [Fig. 8(a), solid line] cross over from SE to PA within one ps after photoexcitation. The crossover can be characterized by an exponential with a 500 fs time constant. For time delays from 1 ps to 1 ns, the decay dynamics at 2.25 eV (SE) and 2.02 eV (PA_{CS}) match exactly. The change of sign from SE to PA, and the exact match of dynamics after 1 ps demonstrate that the SE is completely overwhelmed by PA_{CS} in this material. The existence of SE for the first ps after photoexcitation leads to the conclusion that PA_{CS} is not directly photogenerated, but evolves through an indirect process occurring on the time scale of 1 ps at these pump fluences.

Figure 8 (b) shows the dynamics of PA_{CS} for pump fluences of 10^{14} (dashed line) and 10^{15} (solid line). These dynamics are clearly independent of pump fluence over this range, in stark comparison to the dynamics of PA_{EX}, which vary strongly in going from 10^{13} to $10^{14}\,\mathrm{cm}^{-2}$ [Fig. 8 (a)]. In addition, the picosecond scale dynamics of PA_{EX} and PA_{CS} are plotted together in the inset to Fig. 8(b); the dynamics of PA_{EX} are clearly faster than for PA_{CS}. These results are similar to those obtained for PFO and MEH-DSB films.

The intensity dependence of PA_{EX} is compared to that of PA_{CS} (taken at 2.02 eV, the spectral position where the TA signal crosses zero at the zero time delay due to the exact cancellation of SE and PA_{EX}) in Fig. 9. Both measurements were taken at the peak of the TA signal. The results are identical to those obtained for PFO (see Fig. 5). We find again that PA_{EX} is linear in pump fluence up to a fluence of

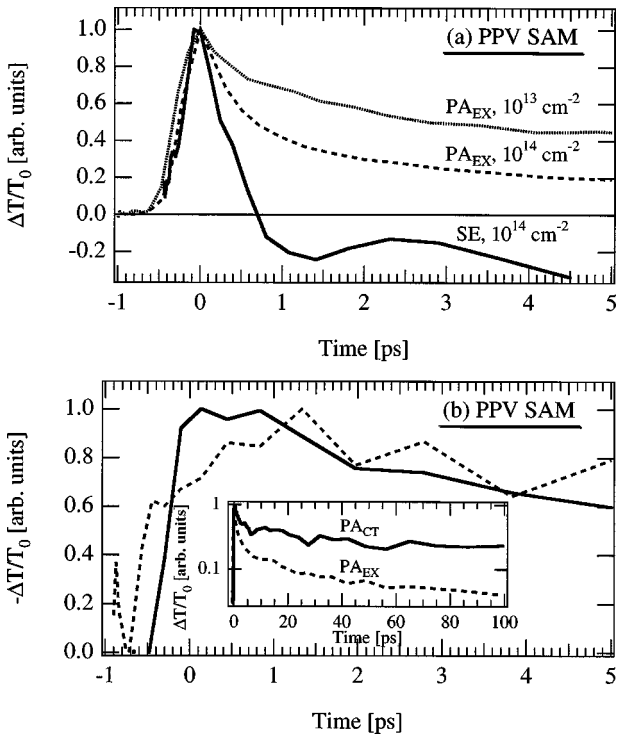

FIG. 8. Panel (a) shows the dynamics of the SE (solid line) at a pump fluence of $10^{14}\,\mathrm{cm}^{-2}$, and of PA_{EX} at a pump fluence of 10^{13} (dotted line) and $10^{14}\,\mathrm{cm}^{-2}$ (dashed line). Panel (b) shows the dynamics of PA_{CS} (1.9 eV) at a pump fluence of 10^{14} (dashed line) and 10^{15} (solid line) cm^{-2}. The inset to panel (b) compares the dynamics of PA_{EX} (dashed line) with those of PA_{CS} (solid line) for a pump fluence of $10^{14}\,\mathrm{cm}^{-2}$.

$\sim 10^{15}\,\mathrm{cm}^{-2}$, at which point saturation begins, and PA_{CS} is precisely quadratic with respect to PA_{EX}, both above and below the saturation point. Hence PA_{CS} in PPV SAM's is generated through a mechanism that is quadratic in the exciton population.

In materials where PA_{CS} does not compete so strongly with the SE, the exact match of the dynamics of the SE and

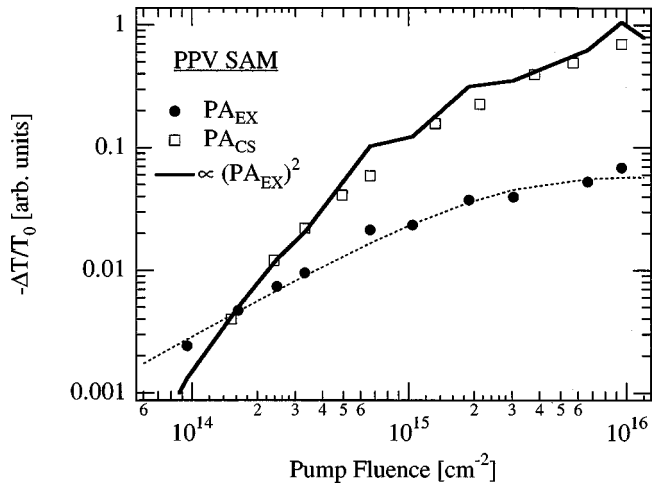

FIG. 9. The pump-fluence dependence of PA_{EX} (solid circles) and of PA_{CS} (open squares) in PPV SAMs at the peak of the TA signal. The heavy-solid line is the (scaled) square of the data for PA_{EX}, and the thin-dashed line is a fit using equation (1), and yields a saturation fluence of $\sim 10^{15}\,\mathrm{cm}^{-2}$.

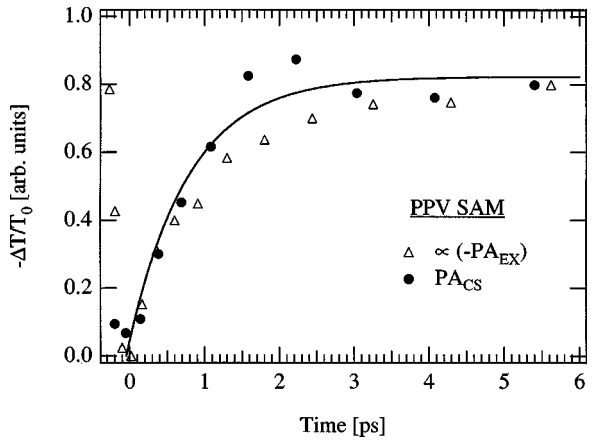

FIG. 10. The growth dynamics of PA_{CS} (solid circles) and the decay dynamics of PA_{EX} (open triangles) in PPV SAMs for a pump fluence of $10^{15}\,\mathrm{cm}^{-2}$. The decay dynamics have been inverted and scaled to highlight the complementary dynamics between the growth of the PA_{CS} and the decay of PA_{EX}. The thin-solid line is a momoexponential fit to the growth dynamics of PA_{CS} and yields a time constant of ~ 800 fs.

PA_{EX} proves that PA_{EX} is due to singlet intrachain excitons. In PPV SAM's PA_{CS} strongly overlaps the SE, preventing a direct comparison of the dynamics of the SE and PA_{EX}. However, the initial fast decay of PA_{EX} is found to be complementary to the risetime of PA_{CS} (see Fig. 10, $\tau_{rise} = 800$ fs), as was observed in PFO, and which is also found in all of the materials where there is negligible overlap between SE and PA_{CS} (see below). This fact, combined with the identical quadratic relationship between PA_{EX} and PA_{CS} in PPV SAM's as is found in the other materials, leads us to conclude that PA_{EX} in PPV SAM's is also due to singlet intrachain excitons.

In general, we find that the photophysics of PPV SAM's are very similar to those of PFO and of MEH-DSB, with a PA_{EX} band peaking in the near-IR, and a PA_{CS} band that peaks in the spectral region between the SE and the PA_{EX} band, that depends quadratically on the intensity of the PA_{EX} band and whose growth rate is identical to the initial fast decay of PA_{EX}.

C. MPS-PPV solutions

The TA spectrum of a 10^{-3} M solution of MPS-PPV in water is plotted in Fig. 11 for a pump-probe delay time of 0.1 ps, using a pump fluence of $10^{14}\,\mathrm{cm}^{-2}$. The different spectral regions have again been labeled as PA_{EX}, PA_{CS}, and SE, with the spectral positions of the measurements of the dynamics and pump-fluence dependence for these features indicated by arrows. The spectra show the same general features as reported in the spectra discussed above for PFO films, MEH-DSH films and PPV SAMs. In this material we also find that the zero-crossing point of the TA spectra undergoes a ''blueshift'' during the first 2 ps, similar to what was observed in the PPV SAMs.

The inset to Fig. 11 shows the TA difference band, which was obtained as discussed above for PPV SAM's, by subtracting the zero-time spectrum from the scaled spectrum at 2 ps. The result shows that within 2 ps of photoexcitation, a

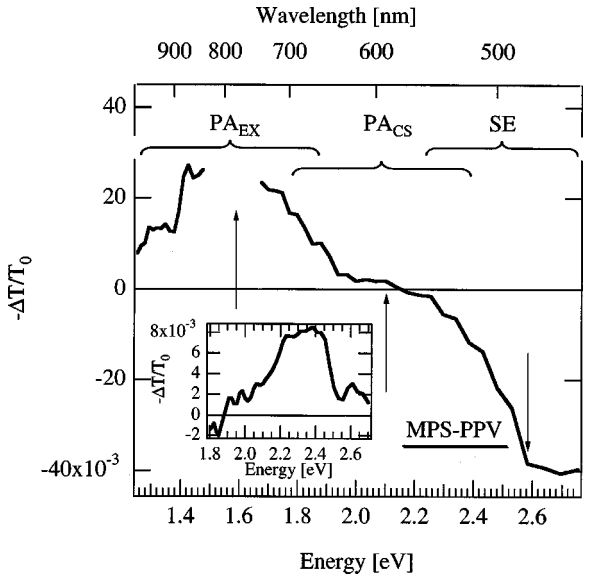

FIG. 11. The chirp-free transient absorption spectrum of MPS-PPV in water at a pump-probe delay time of 0.1 ps taken using a pump fluence of $5\times10^{13}\,\mathrm{cm}^{-2}$. The arrows mark the regions where measurements of the dynamics were taken, and spectral regions of PA_{EX}, PA_{CS}, and the SE are indicated. The inset shows the difference spectrum, which is the result of scaling the 2 ps spectrum so that it matches the 0.1 ps spectrum in the region of SE, then subtracting the 0.1 ps spectrum from the (scaled) 2 ps spectrum.

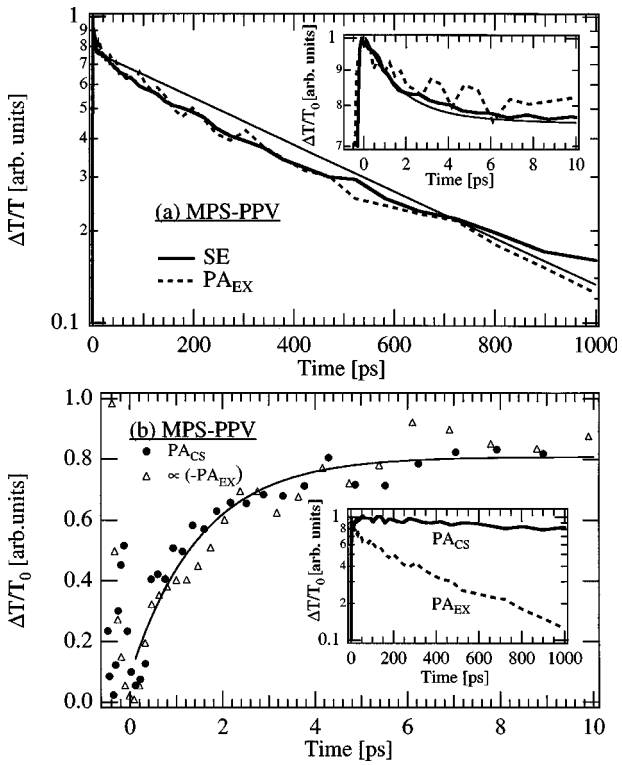

FIG. 12. Panel (a) shows the dynamics of the SE (heavy solid line) and PA_{EX} (dashed line) for MPS-PPV. The thin-solid lines is a fit using a biexponential, and yields time constants of 500 ps and 1.5 ps. The inset to panel (a) shows the same data (and fit) up to a 10 ps pump-probe delay time. Panel (b) shows the dynamics of PA_{CS} (solid circles) and the dynamics of the PA_{EX} (open triangles), inverted and scaled. The thin-solid line is a momoexponential fit to the growth dynamics of PA_{CS} and yields a time constant of $\sim$1.5 ps. The inset to panel (b) shows the ns scale dynamics of PA_{CS} (solid line) and PA_{EX} (dashed line) at the same pump fluence.

secondary (PA_{CS}) band has emerged. The spectrum of this difference band is similar to the spectrum of PA_{CS} observed (or extracted by difference spectra) for all of the phenylene-based materials in this paper.

The dynamics of PA_{EX} and the SE in the MPS-PPV solution are identical on all time scales [Fig. 12(a)], demonstrating that the same species (singlet intrachain excitons) are responsible for both features. The thin-solid line in Fig. 12(a) is a fit to a double exponential, and shows that the decay dynamics contain two time constants: 1.5 and 570 ps. The time constant of 570 ps is typical of radiative time constants of PPV derivatives in solution.[36] The 1.5 ps initial decay corresponds exactly to the growth time of PA_{CS}, as shown in Fig. 12(b), which displays the SE dynamics inverted and scaled to match the growth of PA_{CS}. As observed for PPV SAMs and MEH-DSB films, the PA_{CS} feature competes directly with the SE, but in this case the relative magnitude of the PA_{CS} feature is much smaller than for the two other materials in thin film form. This is consistent with the interpretation that a fraction of the MPS-PPV solution is aggregated, with interchain interactions similar to those observed in thin films, but that this fraction is relatively smaller than for films.

The MPS-PPV solutions represent an intermediate case between the dilute solutions of MEH-DSB studied previously, and the thin films of other materials. The growth of the PA_{CS} feature is clearly associated with aggregation of the polymer in the solutions. This conclusion is strengthened by TA measurements in a more dilute MPS-PPV solution (4×10^{-4} M). In this more dilute solution, a PA_{CS} feature can still be discerned, but its relative magnitude (compared to those of SE and PA_{EX}) is reduced. Interestingly, no intensity-dependent dynamics were observed for either PA bands or SE in either of the solutions, up to the highest pump fluences used. Despite relatively strong interchain interactions and aggregation, there is no evidence of nonlinear decay in these solutions. This is consistent with both bimolecular annihilation and amplified spontaneous emission as mechanisms for nonlinear decay. Both of these effects depend on the volume excitation density (photons absorbed per cm^3), which is much lower for partially aggregated solutions than for solid films using similar pump fluences.

The ns scale dynamics of PA_{CS} and PA_{EX} are shown in the inset to Fig. 12(b). The decay of PA_{CS} in this experiment may be characterized with using a monoexponential with a time constant of 5 ns. Clearly, in view of the limited dynamic range of the measurement, this result is not definitive. However, it is clear that the species responsible for PA_{CS} is much longer-lived than the singlet intrachain exciton. This trend is observed in all the materials discussed in this work.

Finally, we show the pump-fluence dependence of the peak of the TA signal for PA_{CS} and PA_{EX} in Fig. 13. Fitting the data for PA_{EX} using Eq. (1), we again find that PA_{EX} is linear in pump fluence up to a saturation fluence. Since only the relative pump fluence was measured in this experiment, the exact fluence at which saturation occurs is unknown. However, PA_{CS} again is exactly quadratic with respect to PA_{EX} both above and below the saturation point of PA_{EX}.

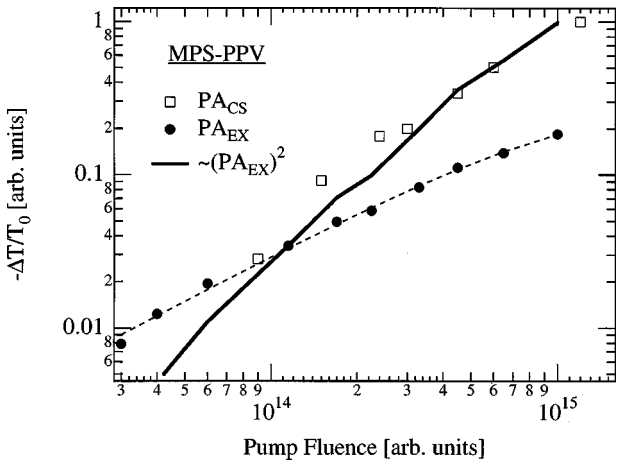

FIG. 13. The pump-fluence dependence of PA_{EX} (solid circles) and of PA_{CS} (open squares) in MPS-PPV at the peak of the TA signal. The heavy-solid line is the (scaled) square of the data for PA_{EX}, and the thin-dashed line is a fit using Eq. (1).

D. DP6-PPV films

The chirp-free TA spectrum taken at ~ 0.1 ps pump-probe delay time for DP6-PPV is shown in Fig. 14, for an excitation density of $10^{14}\,\mathrm{cm}^{-3}$. The spectrum is similar to that observed in the previously discussed materials, with strong SE from 2.1 to 2.7 eV, and broad PA at lower energies.

As with the previous samples studied, the different intensity-dependent dynamics of the PA_{EX} and PA_{CS} bands allow us to identify two different photoexcited species, which contribute to the overall PA in pristine DP6-PPV. The dynamics of the SE are displayed in Fig. 15(a) for excitation densities of 10^{13} (solid circles), 10^{14} (solid triangles), and $10^{15}\,\mathrm{cm}^{-2}$ (solid squares). The dynamics of PA_{EX} are also plotted in Fig. 15(a) (thin-solid lines) for the same pump fluences. PA_{EX} and SE match exactly at all pump fluences, demonstrating again that the two features arise from the same species (singlet intrachain excitons). In addition, the results indicate a pronounced dependence of the dynamics on the excitation density, progressing from monoexponential at the lowest pump fluences (time constant ~ 300 ps), to strongly nonexponential at the highest pump fluences.

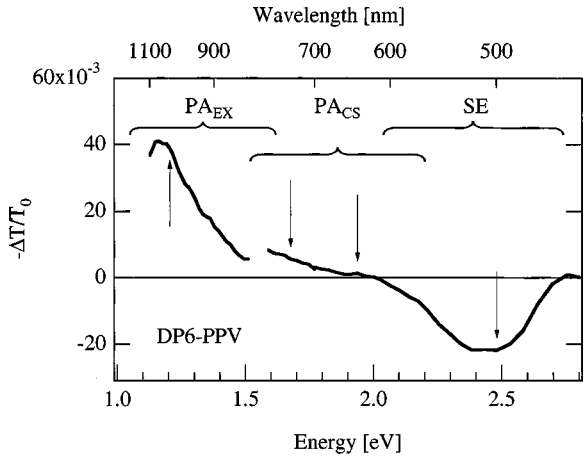

FIG. 14. Panel (a) shows the chirp-free transient absorption spectrum of DP6-PPV at 0.1 ps pump-probe delay time taken with a pump fluence of $3\times 10^{14}\,\mathrm{cm}^{-2}$. The arrows mark the regions where the dynamics and pump-fluence dependence were measured, and spectral regions of PA_{EX}, PA_{CS}, and the SE are indicated.

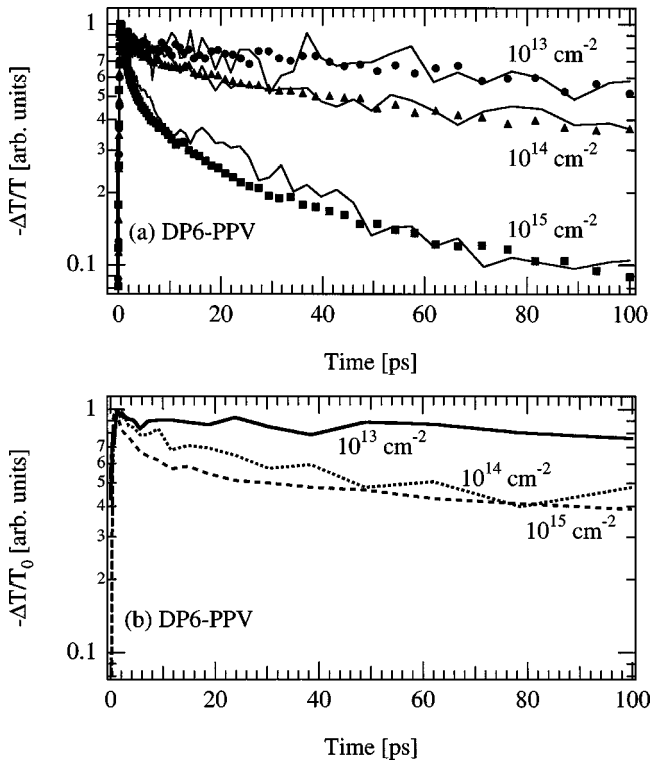

FIG. 15. Panel (a) shows the dynamics of the SE for DP6-PPV for a pump fluence of 10^{13} (solid circles), 10^{14} (solid triangles) and 10^{15} (solid squares) cm^{-2}. The thin-solid lines are the dynamics of PA_{EX} at the same pump fluences. Panel (b) shows the dynamics of PA_{CS} for pump fluences of 10^{13} (solid line), 10^{14} (dotted line), and 10^{15} (dashed line) cm^{-2}.

The dynamics of PA_{CS} are shown in Fig. 15(b) for excitation densities of 10^{13} (solid line), 10^{14} (dotted line), and $10^{15}\,\mathrm{cm}^{-2}$ (dashed line), and display a much less pronounced dependence on excitation density than observed for PA_{EX}, in accordance with the results for the other materials. In addition, as was the case for the previous samples, the long-time dynamics of PA_{CS} are significantly slower than those of PA_{EX} at all pump fluences, indicating that the species that gives rise to PA_{CS} is longer-lived than the singlet exciton.

The peak of the TA signal for the PA_{EX} feature is linear in pump fluence, until saturation occurs at an excitation density of $\sim 10^{15}\,\mathrm{cm}^{-2}$ (see Fig. 16). PA_{CS} is again quadratic with respect to PA_{EX}, both above and below saturation of PA_{EX}. Also, the growth dynamics of PA_{CS} again are complementary to the initial fast decay of PA_{EX} (see Fig. 17). For this material, we find $\tau_{rise}=350$ fs. We are thus led to the same picture of the photophysics of pristine DP6-PPV as for the three previous materials reported above, namely that singlet excitons are responsible for PA_{EX} and that the charge-separated species is created at the expense of singlet excitons via a quadratic process.

E. Photodegraded and C_{60}-doped DP6-PPV films

In this subsection we give the results for films of DP6-PPV that have been either intentionally photodegraded or doped (1:1 M) with the soluble fullerene derivative PCBM.

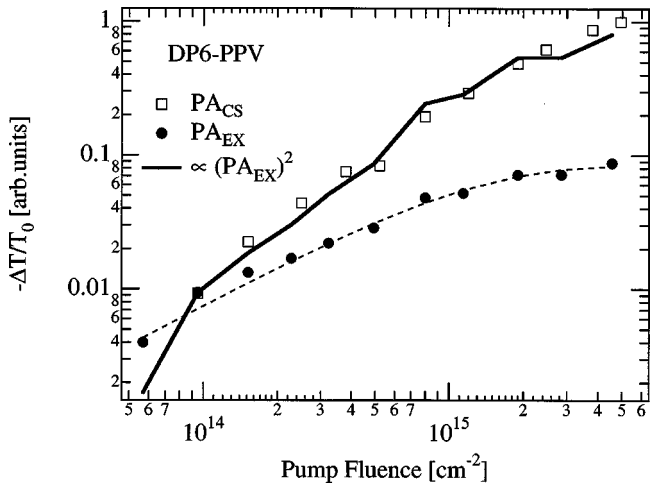

FIG. 16. The pump-fluence dependence of PA_{EX} (solid circles) and of PA_{CS} (open squares) in DP6-PPV at the peak of the TA signal. The heavy-solid line is the (scaled) square of the data for PA_{EX}, and the thin-dashed line is a fit using Eq. (1), and yields a saturation fluence of $\sim 10^{15}\,\mathrm{cm}^{-2}$.

In both cases, we are increasing the density of electron accepting sites in the material as compared to the pristine material, either through the formation of terminal carbonyl and aldehyde groups (for the case of photodegradation) or through direct injection of electron accepting molecules (for the case of C_{60} doping).

The subpicosecond TA spectra of DP6-PPV/C_{60} (1:1 M) for a pump fluence of $10^{14}\,\mathrm{cm}^{-2}$ is shown in Fig. 18(a) (solid line) along with the TA spectra of pristine DP6-PPV for comparison. The spectra for the pristine material are for pump fluences of 10^{13} (dashed line) and $10^{15}\,\mathrm{cm}^{-2}$ (dotted line), normalized to the peak of the SE for ease of comparison. Below the saturation density for PA_{EX}, the zero crossing of the TA spectrum in pristine DP6-PPV does not shift significantly in time—in this regime there is negligible time-dependent competition between SE and PA. However, at the saturation density for PA_{EX}, the zero-crossing of the TA spectrum begins to shift towards the blue. In the doped sample, the PA_{CS} band dominates the TA spectrum, pushing the zero crossing of the TA spectrum approximately 300 meV towards the blue as compared to the pristine sample at a similar pump fluence. The subpicosecond TA spectra of photodegraded and pristine samples are plotted over a broader spectral range in the inset to Fig. 18(a).

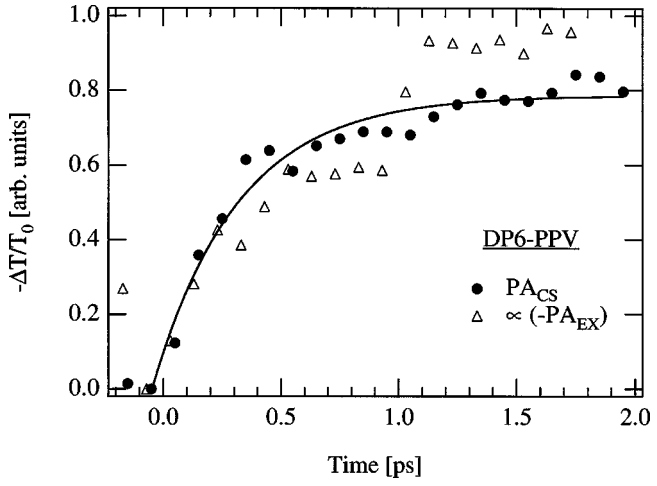

FIG. 17. The growth dynamics of PA_{CS} (solid circles) and the decay dynamics of PA_{EX} (open triangles) in DP6-PPV for a pump fluence of $10^{15}\,\mathrm{cm}^{-2}$. The decay dynamics have been inverted and scaled to highlight the complementary dynamics between the growth of the PA_{CS} and the decay of PA_{EX}. The thin-solid line is a momoexponential fit to the growth dynamics of PA_{CS} and yields a time constant of $\sim$350 fs.

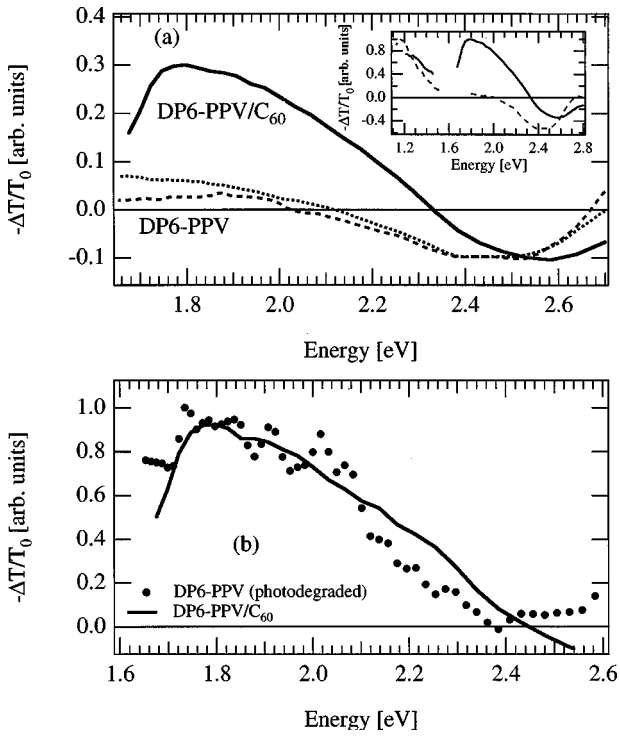

FIG. 18. Panel (a) shows the TA spectrum of ''pristine'' DP6-PPV at <1 ps pump-probe delay time for a pump fluence of 10^{13} (dashed line) and 10^{15} (dotted line) cm^{-2}. The solid line shows the TA spectrum of intentionally photodegraded DP6-PPV at <1 ps pump-probe delay time for an excitation density of $10^{14}\,\mathrm{cm}^{-2}$. The spectra are normalized at 2.5 eV for ease of comparison. The inset to panel (a) shows the TA spectrum at <1 ps pump-probe delay time of the intentionally photodegraded sample out to 1.2 eV (solid line) and the normalized spectrum of ''pristine'' DP6-PPV for comparison (dashed line). Panel (b) shows the early-time TA spectrum of photodegraded DP6-PPV (solid circles) and of DP6-PPV/C_{60} (1:1 M, solid line) using a pump fluence of $10^{14}\,\mathrm{cm}^{-2}$. These spectra are normalized to one at 1.8 eV for ease of comparison.

The subpicosecond TA spectrum of intentionally photodegraded DP6-PPV is shown in Fig. 18(b) (solid circles), along with the subpicosecond TA spectrum of DP6-PPV/C_{60}. Clearly the two spectra are identical, implying that PA_{CS} is not affected by the nature of the electron accepting species.

The dynamics of PA_{CS} in the pristine material also closely match the dynamics of PA_{CS} in both the intentionally photodegraded material and in the C_{60}-doped material, as shown in Fig. 19. This is in agreement with the results of Denton *et al.*, who observed that the TA dynamics in the spectral region we have assigned as PA_{CS} were identical for both oxidized and pristine PPV films.[33] In addition, we find that the risetime of PA_{CS} is still complementary to the initial fast

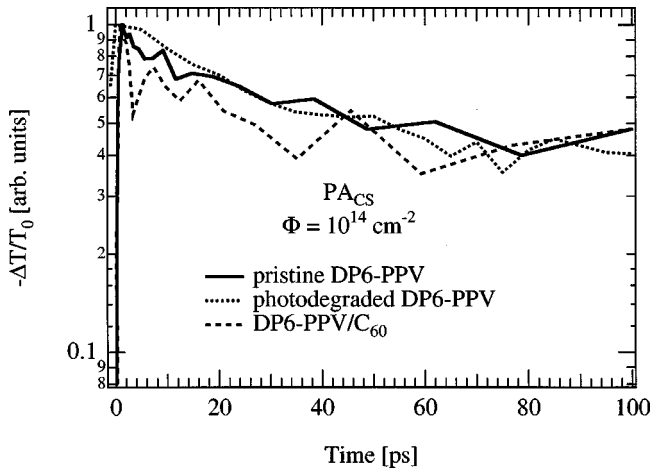

FIG. 19. The dynamics of PA_{CS} in pristine DP6-PPV (solid line), photodegraded DP6-PPV (dotted line) and DP6-PPV/C_{60} (1:1 M, dashed line) for a pump fluence of $10^{14}\,cm^{-2}$.

decay of PA_{EX} in DP6-PPV/C_{60} (see Fig. 21), as was the case for the pristine material. The rise time in this case is $\tau_{rise}=700$ fs. The fact that the rise-time is slower than was found for the pristine material is attributed to the higher pump fluences used in the former case. This is necessary since PA_{EX} dominates PA_{CS} in the pristine material, so that PA_{CS} must be measured near the zero crossing of the TA spectrum in order to avoid the spectral overlap of PA_{EX}. In the doped material, PA_{CS} dominates the TA spectrum, and hence may be measured at its peak so that high pump fluences are not required in order to achieve a reasonable signal-to-noise ratio.

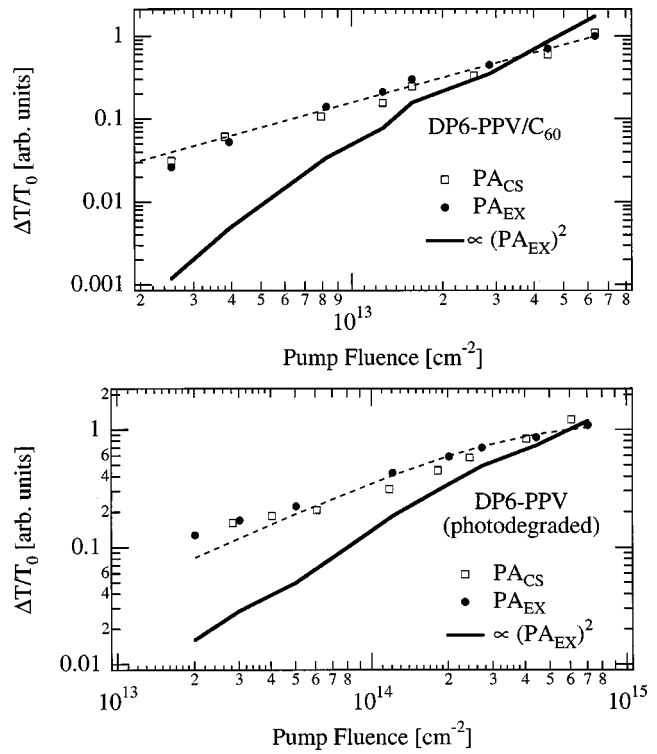

FIG. 20. The dependence of PA_{EX} (solid circles) and of PA_{CS} (open sqares) on pump fluence at the peak of the TA signal for DP6-PPV/C_{60} (panel a) and for photodegraded DP6-PPV (panel b). The dashed line is a fit using Eq. (1), and the solid line is the scaled square of the data for PA_{EX}.

Finally, in comparing the dependence of PA_{EX} and PA_{CS} on pump fluence for photodegraded or doped DP6-PPV with the results presented above for all the pristine materials, we find a striking difference: PA_{CS} is no longer quadratic with respect to the exciton density, but is now *linear* (see Fig. 20).

F. Summary of results

Thus, in all four phenylene-based polymers studied here, we observe a TA feature peaking in the near-IR (PA_{EX}) whose dynamics are strongly intensity dependent and match those of the SE over several orders of magnitude in pump fluence. This feature (PA_{EX}) is attributed to a transition of the primary singlet exciton to a higher excited state. A second TA feature is also observed in all the materials studied (PA_{CS}) peaking in the region between PA_{EX} and the SE. We will discuss the assignment of this second feature in detail below.

The picosecond scale dynamics of PA_{CS} are essentially independent of the initial excitation density and are much slower than the dynamics of PA_{EX}. In all materials we find that the peak TA signal of PA_{EX} is linear in pump fluence, while the intensity dependence of PA_{CS} is sample-dependent. In pristine materials with a low degree of degredation PA_{CS} is quadratic with respect to PA_{EX}, whereas in photodegraded materials or materials doped with C_{60}, PA_{CS} is linear with respect to PA_{EX}. In all cases we find that the risetime of PA_{CS} is complementary to the initial fast decay of the singlet excitons, implying that in all the materials studied here these excitations are created at the expense of singlet excitons.

IV. DISCUSSION

The related TA spectral features and dynamics in each of the phenylene-based materials presented above indicate that two types of excitations are created in all of these materials: the primary intrachain singlet exciton (responsible for the PA_{EX} and SE bands), and a secondary species associated with strong intermolecular interactions (responsible for the PA_{CS} band). There is now wide agreement about the properties of the primary singlet excitons. However, while many authors have investigated the secondary species, their properties (and whether these properties are particular to a given sample, or general to the entire family) remain controversial. In this section, we examine in more detail the precise nature of the secondary species, and the mechanisms of their generation. We first discuss possible contributions to PA_{CS} by excimers, spatially-indirect excitons (polaron pairs), and polarons formed from excitons through electron transfer at electron-accepting defects and dopants. In addition, we address the contributions of generation processes that are both linear and nonlinear in exciton density.

A. Nature of the secondary photoexcitations in phenylene-based polymers and oligomers

The fact that the species responsible for PA_{CS} are created only in samples with relatively strong intermolecular interactions indicates that either the excited state wave function is spread over two or more molecules (such as excimers or

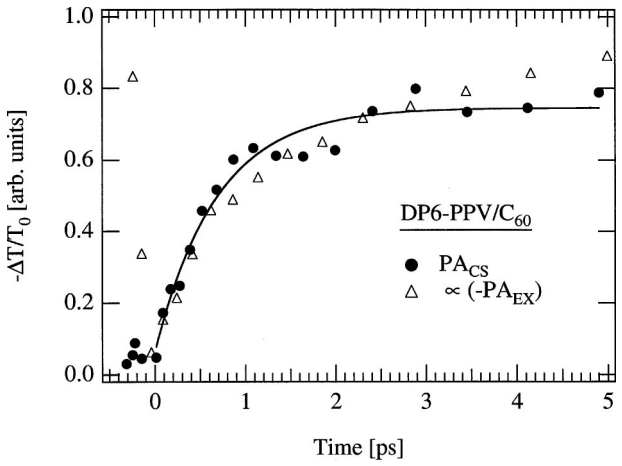

FIG. 21. The growth dynamics of PA_{CS} (solid circles) and the decay dynamics of PA_{EX} (open triangles) in DP6-PPV/C_{60} for a pump fluence of $10^{15}\,cm^{-2}$. The decay dynamics have been inverted and scaled to highlight the complementary dynamics between the growth of the PA_{CS} and the decay of PA_{EX}. The thin-solid line is a momoexponential fit to the growth dynamics of PA_{CS} and yields a time constant of $\sim$700 fs.

polaron-pairs) or that the formation process of the species involves two moieties (such as exciton dissociation into polarons via charge transfer at defects or dopants).[21,57] Regardless of the exact nature of the excited state, this evidence points to an increased charge separation in comparison to the neutral intrachain exciton, and hence we have assigned the secondary photoexcitations as charge-separated excitations.

Although this assignment is noncontroversial, the exact nature of the charge-separated excitations is still subject to debate. In their initial work, Rothberg and co-workers assigned this species to polaron pairs.[20,21] More recently, this assignment has been revised, and recent work concludes that the secondary species are excimers (this revised interpretation was based primarily on spectrally and temporally resolved photoluminescence measurements).[35]

An excimer is defined as an excited dimer which is dissociative in the ground state.[58] The wave function of an excimer is characterized by resonance contributions of both charge transfer and neutral exciton wavefunctions.[59] The most complete understanding of the coupling of molecular excitons on adjacent molecules has come from the study of small oligomers such as stilbenes, azobenzenes, and related compounds.[60–63] The most comprehensive work has been done in solution and in Langmuir monolayers of chromophores at a water surface or in supported Langmuir-Blodgett multilayers. By incorporating the chromophore into a fatty acid structure, one can obtain a preferred orientation of the chromophore, which pack in unique ways as the monolayer is spread and subsequently compressed at the air-water interface. As the concentration of molecules on the surface is increased by decreasing the surface area, the chromophores begin to interact, dictated both by the molecular structure and the packing geometry. For example, for the stilbenes and azobenzenes, the molecules pack preferentially in an ''edge-to-face'' geometry (leading in an extended array to a *herringbone lattice*).[60,61] In this arrangement, the π electrons on adjacent monomers interact most strongly, leading to a mixing of exciton states, a large blue-shift of the absorption, and a symmetric redshift of the emission. For other chromophores such as styrenes, or for stilbenes in which one of the phenyl units is replaced by an α-naphthyl group, ''face-to-face'' packing is favored instead in tightly packed monolayers (leading in an extended array to a *translation lattice*), with smaller (but still significant) spectral shifts. These excimers are substantially less emissive than excitons, due to a lower transition probability (nearly forbidden symmetry for dipole transitions) of the lower energy excimer excited state.

Excimer formation has been reported to be favorable in conjugated polymers in the case of co-facial ''sandwich'' packing of the polymer unit cells, with intermolecular distances in the range of 3–4 Å .[59] Since the ground state of the excimer is that of the isolated polymer or oligomer molecules, excimer formation naturally follows from the photoexcitation of singlet intrachain excitons in solids or aggregated liquids with the appropriate intermolecular packing. Thus excimers in these systems are expected to form at the expense of the singlet intrachain excitons, localized at positions of close interchain packing or crossing. This is consistent with the evolution of the PA_{CS} feature in the phenylene-based materials in our work. In each of these materials, PA_{CS} forms with a rise time exactly complementary to the initial fast decay of PA_{EX} and SE. However, the formation of excimers would be expected to lead to a linear dependence of the magnitude of PA_{CS} on excitation density;[35] we observe that the peak PA_{CS} signal scales exactly as the square of PA_{EX} for all four materials studied (provided that the materials are not deliberately doped or degraded).

Interchain polaron-pairs (or spatially indirect excitons) also have been predicted to form at the expense of singlet intrachain excitons, and also may be invoked to explain PA_{CS}.[57,20,21] Charge separation is more complete for polaron pairs than for excimers, making polaron pairs completely nonemissive. Like excimers, polaron pairs would be expected to be strongly localized at the sites of chain crossing, and to recombine geminately, leading to intensity-independent dynamics up to very high excitation densities. Calculations have predicted that the formation of interchain polaron pairs also requires the close proximity of neighboring polymer chains ($\sim$4 Å) over 2 monomers or more,[57] a situation which is certainly possible even in ''amorphous'' samples. Hence, interchain polaron pairs may also contribute to PA_{CS}. However, as for excimers, this process would be expected to lead to linear intensity dependence for PA_{CS}, rather than the observed quadratic dependence.

We now turn our attention to the PA_{CS} signature for films that are known to be dominated by exciton quenching at electron-accepting defects or dopants. Our systematic study of DP6-PPV films is particularly revealing; our samples ranged in a controlled manner from pristine, highly emissive films, to intentionally photodegraded films (weakly emissive), to films doped 1:1 with the fullerene derivative PCBM (nearly nonemissive). In each case, the spectral signature and dynamics of the PA_{CS} feature are identical (Fig. 18 and Fig. 19); this feature simply becomes more prominent. In the case of the fullerene-doped films and the highly degraded films, the SE disappears completely within 1 ps of photoexcitation. In addition, PA_{CS} changes from quadratic to linear in pump fluence (Fig. 20) and the growth of PA_{CS} is exactly comple-

mentary to the initial fast decay of PA_{EX} (Fig. 21), implying linear generation of the secondary excitations from the primary excitons. It is known that in photo-oxidized PPV films, excitons are dissociated by electron transfer to carbonyl defects (created photochemically at the expense of the vinylene double bonds).[24,26,33,43,44] Similar ultrafast electron transfer has been reported for other PPV derivatives mixed with small amounts of C_{60},[64] leading to a modified PA spectrum similar to that reported here for oxidized and fullerene-doped films of DP6-PPV. Hence, we attribute the PA_{CS} feature in DP6-PPV to charge transfer polarons: polarons which are formed upon electron transfer to a defect or dopant. *The identical spectral shape and dynamics for the* PA_{CS} *feature in photo-oxidized and fullerene-doped films suggests that this feature is not related to the electron trapping site, but rather is a signature of the hole polaron remaining on the polymer after exciton dissociation and electron transfer.* Hence, the assignment of PA_{CS} to hole polarons seems unambiguous in films in which excitons are known to undergo fast and efficient electron transfer.

However, we stress the fact that the spectral shape and dynamics of PA_{CS} are similar over the whole range of materials studied, including pristine samples of DP6-PPV, MPS-PPV, PFO, PPV SAMs, and MEH-DSB. In these materials, charge transfer polarons may be expected to play a smaller role (thus, the relative contributions of excimers and/or polaron pairs should be greater). In particular, since PFO does not contain a vinylene double bond, it is not expected to suffer from the same photodegradation mechanism as the PPV derivatives. Indeed, under our experimental conditions, PFO is much more photo-stable in air than PPV and its derivatives.

The generation efficiency and electronic structure of both excimers and interchain polaron pairs has been shown theoretically and experimentally to depend sensitively on such extrinsic factors as intermolecular packing geometry and the spatial separation between adjacent chains. The spectral position of PA_{CS}, if due to these species, should shift as the excited-state energy of the excimer or polaron pair shifts in response to changes in coupling of the molecular excitonic states. It is difficult to rationalize that the end result would be the same in all of the samples studied here, which due to the very different side chains are expected to display a large variation in interchain interactions. The signature of charge transfer polarons, on the other hand, should not be as sensitive to sample morphology.

We are thus led to the interpretation that the PA_{CS} spectral feature is in all cases due to polarons created from excitons via charge transfer to a dopant or defect, or via interchain charge transfer in pristine materials. One well-documented effect of C_{60}-doping on PPV derivatives is an increase by several orders of magnitude of the transient and CW photoconductivity, due to the efficient generation of mobile charge carriers (hole polarons). These mobile hole polarons must be distinguished from polaron pairs and excimers which are bound strongly to sites with strong interchain interaction. Similarly, charge transfer polarons which remain tightly bound to the electron trapping site cannot lead to such dramatic increases in photoconductivity. The assignment of PA_{CS} to polarons is attractive, in that only one type of excitation need be invoked to explain the common PA_{CS} spectral feature which extends across the whole family of materials. It may be that the excimer states, if created, do not show strong excited-state transitions in the visible spectral range, due to a reduced transition dipole moment to the available higher states (similar to the reduced transition moment for the radiative transition back to the ground state). In this way, the only excitations that would lead to strongly allowed transitions would be the polarons created on adjacent chains due to interchain contact or electron transfer.

The only seeming difficulty with this assignment is the observed lack of intensity-dependent dynamics, which has been used to infer a strongly localized, noninteracting species which recombines geminately.[21] However, if only one type of carrier (the electron) is localized (as a result, for example, of deep trapping at a defect or dopant) then the probability of bimolecular annihilation processes for delocalized holes is still significantly reduced: annihilation requires both an electron and a hole. *Hence, the lack of intensity-dependent dynamics may be taken as evidence only that one type of carrier is localized, not necessarily the electron-hole pair.* More generally, once a polaron pair has been created on adjacent chains, long-range dipole-coupled annihilation (e.g., Förster interactions) is suppressed because there is no matrix element coupling the separated electron and hole back to the ground state. Hence, one should expect a higher threshold for nonlinear interactions for interchain polarons than for excitons on general grounds. In our studies, the threshold for bimolecular interactions of excitons is $\sim 10^{15}\,\mathrm{cm}^{-2}$, while the threshold for PA_{CS} is at least an order of magnitude higher.

B. Generation mechanisms for the secondary photoexcitations in phenylene-based polymers and oligomers

It has been established that the secondary photoexcitations (leading to the PA_{CS} band) in thin films of the oligomer MEH-DSB are generated via biexciton states.[30,31] This may involve generation of either doubly-excited excitons (biexcitons) through sequential absorption of two photons from the same intense femtosecond pulse, a process believed to be responsible for the subpicosecond generation of triplet excitons in isolated chains of poly(diacetylene) derivatives,[65] or through indirect excitation of singlet excitons to biexcitons through an Auger process involving bimolecular annihilation of singlet excitons. In MEH-DSB films, the intensity-independent rise time of the PA_{CS} band argues in favor of the first of these two generation mechanisms. Once created via either mechanism, if intermolecular interactions permit, the biexciton state may decay to an interchain excitation, giving rise to the PA_{CS} band.

In PFO and PPV SAMs, previous measurements of the intensity-dependent magnitude of the PA at the apparent peak of the PA_{CS} band indicated a linear dependence on pump fluence.[32] However, due to substantial overlap of PA_{EX} and PA_{CS}, the results are ambiguous. An unequivocal measurement of the intensity-dependent magnitude in such a case of overlapping spectral features can only be made at the point where SE and PA_{EX} exactly balance to give a zero net PA signal from the singlet exciton. This wavelength is chosen by determining the zero-crossing point in the earliest time TA spectrum. At this wavelength, the intensity depen-

dence of PA_{CS} is exactly quadratic relative to PA_{EX} for all four polymers used in this work. This result agrees with that reported for MEH-DSB, and implies that the creation of the hole polarons in these materials is also mediated by biexciton states.

The determination of which of the two possible nonlinear generation processes listed above dominates is hindered by the extremely small signal-to-noise ratio, since measurements of PA_{CS} must be made at the zero-crossing of the TA. As a result, it is difficult to measure the rise time of PA_{CS} for pump fluences differing by more than an order of magnitude. Fitting the risetime of PA_{CS} using rate equations describing either sequential absorption or an Auger process works equally well in both cases and therefore also does not help in distinguishing between the two mechanisms. More work is needed to resolve this issue.

Upon doping DP6-PPV with the electron acceptor PCBM the intensity dependence of PA_{CS} (again observed near the zero crossing of the earliest-time ps TA spectrum) becomes linear, identical to that of PA_{EX}, as shown in Fig. 20. The generation mechanism for the hole polarons is therefore linear with respect to exciton density in the doped polymer, contrary to what we observed in the pristine polymers. The importance of this observation must be emphasized. Stated simply, the difference between pristine and doped polymer films is not just the degree of trapping sites available to form polarons. The generation mechanism of charge-separated states is qualitatively different for the two cases. *In pristine samples the formation of these charge-separated states proceeds only via processes that are quadratic with respect to the density of singlet intrachain exitons, while addition of dopants or defects changes this to a process that is mediated by electron transfer to the dopant or defect and which is linear with respect to the exciton density.*

V. CONCLUSIONS

We have presented an extensive study of the transient absorption spectra and dynamics of four different phenylene-based conjugated polymers and an oligomer. Taken together, these results provide powerful evidence that two types of photoexcitations are created, which are general to all five phenylene-based materials studied to date in our laboratory. Because of their generality, we conclude that these excitations form the basis for a unified framework which can be used to understand the photophysics of all phenylene-based conjugated polymeric materials. The two types of photoexcitations detected are the primary intrachain singlet exciton, and a secondary species created at the expense of the excitons, which we attribute to weakly coupled, charge separated (interchain) polarons. In the discussion section, we summarized the properties of these excitations, and attempted to resolve some controversial issues about the precise nature and generation mechanisms for the hole polarons.

The properties of the emissive singlet excitons are now well documented. While these properties have been addressed by many authors for individual members of this family of materials, this work shows conclusively that the TA features of the excitons are common to the entire class of compounds. The main elements are as follows. The singlet intrachain excitons are directly created (<100 fs) following photoexcitation. The new, allowed excited-state transitions lead to strong PA bands, including the PA_{EX} band documented in detail in this work, and another PA band in the near-IR in the vicinity of 0.5 eV.[66] The stimulated transition back to the ground state leads to an SE band, redshifted from the main $\pi-\pi^*$ absorption due to a combination of energy relaxation within an inhomogeneous distribution of emitters, and intrinsic vibronic relaxation (Stokes' shift). These TA spectral features (PA and SE bands) share common dynamics and intensity dependence. The exciton decay is dominated in pristine samples at low-excitation densities by radiative decay with a time constant of order 1 ns. At higher excitation densities, strong nonlinear processes (biexciton generation, exciton-exciton annihilation, and amplified spontaneous emission) lead to rapid depopulation of the excitons either directly to the ground state or to the secondary, charge-separated species. The threshold for the onset of nonlinear relaxation processes is approximately 10^{15} cm^{-2}. This threshold fluence has been used to estimate the spatial extent of the excitons (~ 50 Å), implying an exciton delocalized over many unit cells of the polymer.[41] This is also a typical length scale for dipole-coupled Förster energy transfer processes.

For the secondary species we have examined several potential candidates that have been discussed in the literature: excimers, tightly bound polaron pairs (indirect excitons) and weakly-coupled, charge separated (interchain) polarons. Due to the remarkable similarity of the TA spectrum and dynamics of this secondary spectral feature over a wide range of materials, it is attractive to assign it to a single type of species. By studying films in which it is known that primarily positively-charged (hole) polarons are created due to efficient electron trapping, we attribute this secondary species to hole polarons on the polymer chains. In pristine polymers, the signature may arise from both electron and hole polarons due to near degeneracy of the polaron energy levels. We find that the generation mechanism for polarons is quadratic in exciton density in pristine, undoped polymers, and becomes a linear process in heavily doped or severely photodegraded polymers. The formation time for secondary polarons is material dependent and ranges from the hundred femtosecond regime to several picoseconds for the materials studied in this paper.

ACKNOWLEDGMENTS

We are grateful to many colleagues for agreeing to provide samples that enabled this comprehensive study. MEH-DSB was synthesized by N. Barashkov and J. Ferraris. We thank I. Campbell for the preparation of MEH-DSB samples. PPV-SAM samples were provided by M. Rubner. PPV precursor and DP6-PPV was synthesized and provided by B. Hsieh. PFO samples were provided by D.D.C. Bradley. MPS-PPV and PCBM samples were provided by F. Wudl. This work was supported by Los Alamos National Laboratory Directed Research and Development funds under the auspices of the U.S. Department of Energy.

[1] J. Burroughes, D. D. C. Bradley, A. Brown, R. Marks, K. Mackay, R. Friend, P. Burns, and A. Holmes, Nature (London) **347**, 539 (1990).
[2] D. Braun and A. Heeger, Appl. Phys. Lett. **58**, 1982 (1991).
[3] Q. Pei, G. Yu, C. Zhang, Y. Yang, and A. J. Heeger, Science **269**, 1086 (1995).
[4] F. Hide, M. A. DiazGarcia, B. J . Schwartz, M. R. Andersson, Q. B. Pei, and A. J. Heeger, Science **273**, 1833 (1996).
[5] N. Tessler, G. Denton, and R. Friend, Nature (London) **382**, 695 (1996).
[6] S. Frolov, M. Shkunov, Z. Vardeny, and K. Yoshino, Phys. Rev. B **56**, R4363 (1997).
[7] G. Yu, K. Pakbaz, and A. Heeger, Appl. Phys. Lett. **64**, 3422 (1994).
[8] H. Yu, B. R. Hsieh, M. A. Abkowitz, S. A. Jenekhe, and M. Stolka, Synth. Met. **62**, 265 (1994).
[9] G. Yu, J. Gao, J. C. Hummelen, F. Wudl, and A. J. Heeger, Science **270**, 1789 (1995).
[10] H. Katz, J. Mater. Chem. **7**, 369 (1997).
[11] D. Gundlach, Y. Lin, T. Jackson, and D. Schlom, Appl. Phys. Lett. **71**, 3853 (1997).
[12] H. Sirringhaus, N. Tessler, and R. Friend, Science **280**, 1741 (1998).
[13] A. Dodabalapur, Z. Bao, A. Makhija, J. G. Laquindanum, V. R. Raju, Y. Feng, H. E. Katz, and J. Rogers, Appl. Phys. Lett. **73**, 142 (1998).
[14] D. McBranch and M. Sinclair, in *The Nature of the Photoexcitations in Conjugated Polymers*, edited by N. Sariciftci (World Scientific Publishing, Singapore, 1997).
[15] M. Sinclair, D. McBranch, T. Hagler, and A. Heeger, Synth. Met. **50**, 593 (1992).
[16] R. Kersting, U. Lemmer, R. F. Mahrt, K. Leo, H. Kurz, H. Bässler, and E. O. Göbel, Phys. Rev. Lett. **70**, 3820 (1993).
[17] I. Samuel, F. Raksi, D. D. C. Bradley, R. H. Friend, P. L. Burn, A. D. D. C. Bradley, R. H. Friend, P. L. Burn, A. B. Holmes, H. Murata, T. Tsutsui, and S. Saito, Synth. Met. **55**, 15 (1993).
[18] R. Kersting, U. Lemmer, M. Duessen, H. J. Bakker, R. F. Mahrt, H. Kurz, V. I. Arkhipov, H. Bässler, and E. O. Göbel, Phys. Rev. Lett. **73**, 1440 (1994).
[19] J. Leng, S. Jeglinski, X. Wei, R. E. Benner, Z. V. Vardeny, F. Guo, and S. Mazumdar, Phys. Rev. Lett. **72**, 156 (1994).
[20] J. Hsu, M. Yan, T. M. Jedju, L. J. Rothberg, and B. R. Hseih, Phys. Rev. B **49**, 712 (1994).
[21] M. Yan, L. J. Rothberg, F. Papadimitrakopoulos, M. E. Galvin, and T. M. Miller, Phys. Rev. Lett. **72**, 1104 (1994).
[22] M. Yan, L. Rothberg, B. Hsieh, and R. Alfano, Phys. Rev. B **49**, 9419 (1994).
[23] M. Yan, L. Rothberg, E. Kwock, and T. Miller, Phys. Rev. Lett. **75**, 1992 (1995).
[24] L. Rothberg, F. Papadimitrakopoulos, and M. Galvin, Synth. Met. **80**, 41 (1996).
[25] W. Graupner, G. Leising, G. Lanzani, M. Nisoli, S. DeSilvestri, and U. Scherf, Phys. Rev. Lett. **76**, 847 (1996).
[26] N. Harrison, G. Hayes, R. Phillips, and R. Friend, Phys. Rev. Lett. **77**, 1881 (1996).
[27] J. Blatchford, S. W. Jessen, L. B. Lin, J. J. Lih, T. L. Gustafson, A. J. Epstein, D. K. Fu, M. J. Marsella, T. M. Swager, A. G. Macdiarmid, S. Yamaguchi, and H. Hamaguchi, Phys. Rev. Lett. **76**, 1513 (1996).
[28] B. Schwartz, F. Hide, M. Andersson, and A. Heeger, Chem. Phys. Lett. **265**, 327 (1997).
[29] E. Maniloff, V. Klimov, and D. McBranch, Phys. Rev. B **56**, 1876 (1997).
[30] V. Klimov, D. McBranch, N. Barashkov, and J. Ferraris, Chem. Phys. Lett. **277**, 109 (1997).
[31] V. Klimov, D. McBranch, N. Barashkov, and J. Ferraris, Phys. Rev. B **58**, 7654 (1998).
[32] D. McBranch, B. Kraabel, S. Xu, R. S. Kohlman, V. I. Klimov, D. D. C. Bradley, B. R. Hsieh, and M. Rubner, Synth. Met. **101**, 281 (1999).
[33] G. Denton, N. Tessler, N. Harrison, and R. Friend, Phys. Rev. Lett. **78**, 733 (1997).
[34] I. Samuel, G. Rumbles, C. J. Collison, S. C. Moratti, and A. B. Holmes, Chem. Phys. **227**, 75 (1998).
[35] R. Jakubiak, C. Collison, W. Wan, and L. Rothberg, J. Phys. Chem. **101** (to be published).
[36] T. Nguyen, V. Doan, and B. Schwartz, J. Phys. Chem. **110**, 4068 (1999).
[37] U. Rauscher, H. Bässler, D.D.C. Bradley, and M. Mennecke, Phys. Rev. B **42**, 9830 (1990).
[38] N. Greenham, I. D. W. Samuel, G. R. Hayes, Y. Kessener, S. C. Moratti, A. B. Holmes, and R. H. Friend, Chem. Phys. Lett. **241**, 89 (1995).
[39] R. Kepler, V. Valencia, S. Jacobs, and J. McNamara, Synth. Met. **78**, 227 (1996).
[40] V. Doan, V. Tran, and B. Schwartz, Chem. Phys. Lett. **288**, 576 (1998).
[41] D. Vacar, A. Dogariu, and A. Heeger, Adv. Mater. **10**, 669 (1998).
[42] A. Dogariu, D. Vacar, and A. Heeger, Phys. Rev. B **58**, 10 218 (1998).
[43] M. Yan, L. J. Rothberg, F. Papadimitrakopoulos, M. E. Galvin, and T. M. Miller, Phys. Rev. Lett. **73**, 744 (1994).
[44] D. Sutherland, J. A. Carlisle, P. Elliker, G. Fox, T. W. Hagler, I. Jimenez, H. W. Lee, K. Pakbaz, L. J. Terminello, S. C. Williams, F. J. Himpsel, D. K. Shuh, W. M. WongTong, J. J. Jia, T. A. Calcott, and D. L. Ederer, Appl. Phys. Lett. **68**, 2046 (1996).
[45] F. Wudl, P.-M. Allemand, G. Srdanov, Z. Ni, and D. McBranch, ACS Symp. Ser. **455**, 683 (1991).
[46] P. Burn, A. B. Holmes, A. Kraft, D. D. C. Bradley, A. R. Brown, and R. H. Friend, J. Chem. Soc. Chem. Commun. **101**, 32 (1992).
[47] D. Baigent, A. Holmes, S. Moratti, and R. Friend, Synth. Met. **80**, 119 (1996).
[48] A. Dogariu, D. Vacar, and A. Heeger, Chem. Phys. Lett. **290**, 58 (1998).
[49] R. Tikhoplav and B. Hess, Synth. Met. **101** (to be published).
[50] I. Samuel, G. Rumbles, and C. Collison, Phys. Rev. B **52**, 11 573 (1995).
[51] G. Hayes, I. Samuel, and R. Phillips, Phys. Rev. B **52**, 11 569 (1995).
[52] D. Bradley, M. Grell, A. Grice, A. R. Tajbakhsh, and D. F. Obrien, Opt. Mater. **9**, 1 (1998).
[53] M. Grell, D. D. C. Bradley, X. Long, T. Chamberlain, M. Inbasekaran, E. P. Woo, and M. Soliman, Acta Polym. **49**, 439 (1998).
[54] A. Fou, O. Onitsuka, M. Ferreira, M. F. Rubner, and B. R. Hsieh, J. Appl. Phys. **79**, 7501 (1996).
[55] J. Hummelen, B. W. Knight, F. Lepeq, F. Wudl, J. Yao, and C. L. Wilkins, J. Org. Chem. **60**, 532 (1995).
[56] V. Klimov and D. McBranch, Opt. Lett. **23**, 277 (1998).
[57] H. Mizes and E. Conwell, Phys. Rev. B **50**, 11 243 (1994).

[58] J. Birks, *Photophysics of Aromatic Molecules* (Wiley-Interscience, London, 1970).
[59] S. Jenekhe and J. Osaheni, Science **265**, 765 (1994).
[60] X. Song *et al.*, J. Am. Chem. Soc. **119**, 12 481 (1997).
[61] X. Song, J. Perlstein, and D. Whitten, J. Am. Chem. Soc. **119**, 9144 (1997).
[62] X. Zhao, J. Perlstein, and D. Whitten, J. Am. Chem. Soc. **116**, 10 463 (1994).
[63] L. Chen, C. Geiger, J. Perlstein, and D. Whitten, J. Am. Chem. Soc. (to be published).
[64] B. Kraabel, J. C. Hummelen, D. Vacar, D. Moses, N. S. Sariciftci, A. J. Heeger, and F. Wudl, J. Chem. Phys. **104**, 4267 (1996).
[65] B. Kraabel, D. Hulin, C. Aslangul, C. Lapersonnemeyer, and M. Schott, Chem. Phys. **227**, 83 (1998).
[66] B. Kraabel and D. McBranch (unpublished).